Earth Moon Planets (2012) 108:175–188
DOI 10.1007/s11038-012-9390-2

Modeling the 2.7 km in Diameter, Shallow Marine Ritland Impact Structure

Valery Shuvalov · Henning Dypvik · Elin Kalleson · Ronny Setså · Fridtjof Riis

Received: 11 July 2011 / Accepted: 16 March 2012 / Published online: 4 April 2012

Abstract The newly discovered Ritland impact structure (2.7 km in diameter) has been modeled by numerical simulation, based on detailed field information input. The numerical model applies the SOVA multi-material hydrocode, which uses the ANEOS equation of state for granite, describing thermodynamical properties of target and projectile material. The model displays crater formation and possible ejecta distribution that strongly supports a 100 m or less water depth at the time of impact. According to the simulations resurge processes and basinal syn- and postimpact sedimentation are highly dependent on water depth; in more than 100 m of water depth, much more powerful resurge processes are generated than at water depths shallower than 100 m (the Ritland case). In Ritland the 100 m high (modeled) crater rim formed a barrier and severely reduced the resurge processes. In the case of deeper water, powerful resurge processes, tsunami wave generations and related currents could have triggered even more violent crater fill sedimentation. The presented model demonstrates the importance of understanding the interactions between water layer and both syn-impact crater fill and ejecta distribution. According to the

V. Shuvalov
Institute of the Dynamics of Geospheres, Russian Academy of Sciences, 38 Leninsky Prospect, Building 1, 119334 Moscow, Russia
e-mail: shuvalov@idg.chph.ras.ru

H. Dypvik (✉) · E. Kalleson
Department of Geosciences, University of Oslo, P.O. Box 1047, Blindern, 0316 Oslo, Norway
e-mail: henning.dypvik@geo.uio.no

E. Kalleson
e-mail: elin.kalleson@geo.uio.no

R. Setså
Geoforskning AS, Faculty of Mathematics and Natural Sciences, University of Oslo, P.O. Box 1032, Blindern, 0315 Oslo, Norway
e-mail: ronny@geo.as

F. Riis
Norwegian Petroleum Directorate, P.O. Box 600, 4003 Stavanger, Norway
e-mail: Fridtjof.Riis@npd.no

presented simulations ejecta blocks up to 10 m in diameter could be transported up to about 5 km outside the crater rim.

Keywords Impact craters · Numerical simulation · Modeling · Ritland Crater Norway

1 Introduction

The 2.7 km in diameter Ritland impact structure of southwestern Norway (Figs. 1, 2) is presently a 350 m deep depression partly filled with syn- and early postimpact deposits, consisting of Lower/Middle Cambrian shales and sandstones, and capped by Caledonian nappe units (Riis et al. 2011). The Ritland impact crater was probably formed in the Lower/Middle Cambrian by an impact into the shallow marine waters of the epicontinental sea covering the Fennoscandian shield (Riis et al. 2011). This observation is based on the occurrence of about 10–12 m of marine shales and siltstones below the ejecta outside the crater.

On the mainland of Norway so far only two impact structures have been found; the Ritland and Gardnos structures (Dons and Naterstad 1992; French et al. 1997; Goderis et al. 2009; Kalleson et al. 2008, 2009; Riis et al. 2011). The Ritland and the Gardnos structures are both located on the sub-Cambrian peneplain (Fig. 1), below Cambrian formations. The broad sub-Cambrian peneplain of southern Norway was formed by weathering and erosion through several million years and was later flooded by the Cambrian transgression and buried by sediments. This is a fortunate setting for accumulation and preservation of impact craters. Radiometric dating suggests the Gardnos impact to be 546 ± 5 Ma (Kalleson et al. 2009), while Ritland ejecta recently were documented within Lower/Middle Cambrian dark grey and black shales, indicating a comparable or somewhat younger age (Setså 2011). According to the palaeogeographic reconstructions and stratigraphical compilations of Nielsen and Schovsbo (2006) the target area was dry land through most of the lower Cambrian, with some episodes of flooding. From Middle Cambrian the shallow sea was probably established, with continuous marine sedimentation through the rest of the Cambrian and into the Ordovician. The Ritland impact most likely happened into this shallow epicontinental sea. In the Ritland case we have diagenetic evidence of sporadic carbonate cement of shallow marine origin in addition to stratigraphical evidence by ejecta present within the Lower/Middle Cambrian dark shales (Riis et al. 2011; Kalleson et al. 2012) (Fig. 2). Ejecta have been found in a large area east and north of the structure, outwards to about 5 km outside the crater wall (Setså 2011; Kalleson et al. 2012; Riis et al. 2012). The Ritland crater was probably filled with water a relatively short time after impact (Riis et al. 2011, 2012). Simultaneously with water re-entering the crater cavity slumped material, avalanches, mass flow deposits of coarse grained material of crushed basement fragments built up fans which locally were more than 50 m thick and was eventually covered by suspension flow deposits (Azad et al. 2012) (Fig. 2). A thin, about 2 m, sliver of melt-rocks/suevite is present between the crushed basement and the sedimentary, early post impact successions mentioned (Riis et al. 2011) (Fig. 2). Later, after impact, dark gray clay sedimentation of hypoxic-dominated conditions returned. Today, remnants of this clay are preserved as the dark gray Cambrian shales filling the eastern/southeastern part of the depression and covering parts of the surrounding sub-Cambrian peneplain (about 150 m thick within the structure and 40 m outside). It is hard to estimate how much additional sediments were deposited in Late Cambrian, Ordovician and Silurian times, as most of the overlying sedimentary successions were removed by SE

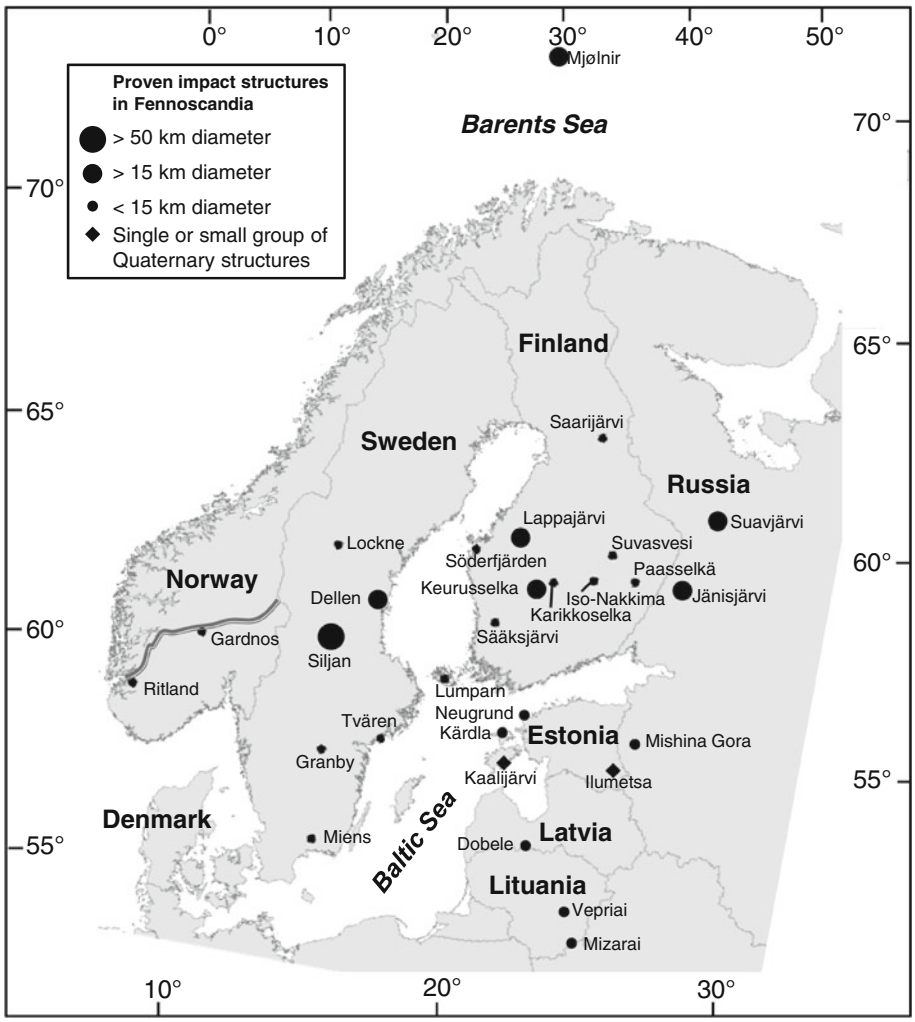

Fig. 1 Geographical map of Northeastern Europe with proven impact structures shown; *dot-size* indicate crater size. The *shaded line* displays the northernmost reach of the sub-Cambrian peneplain in Norway. Modified from Dypvik et al. (2008)

directed thrusting during the Caledonian orogeny. The Caledonian nappe sheets covered the area in late Silurian to Devonian and protected the crater structure for a long period of time, until the last glaciations and postglacial erosion removed the overburden and excavated the present exposures (Riis et al. 2011).

In order to sort out the mechanics of this marine impact event and constrain the geological configuration at the time of impact, we have performed numerical simulations. The modeling contributes to our understanding of crater development and evolution, along with the ejecta formation and its regional distribution given different scenarios of possible water depths. The interaction between the water layer and sediment in the marine impact event is

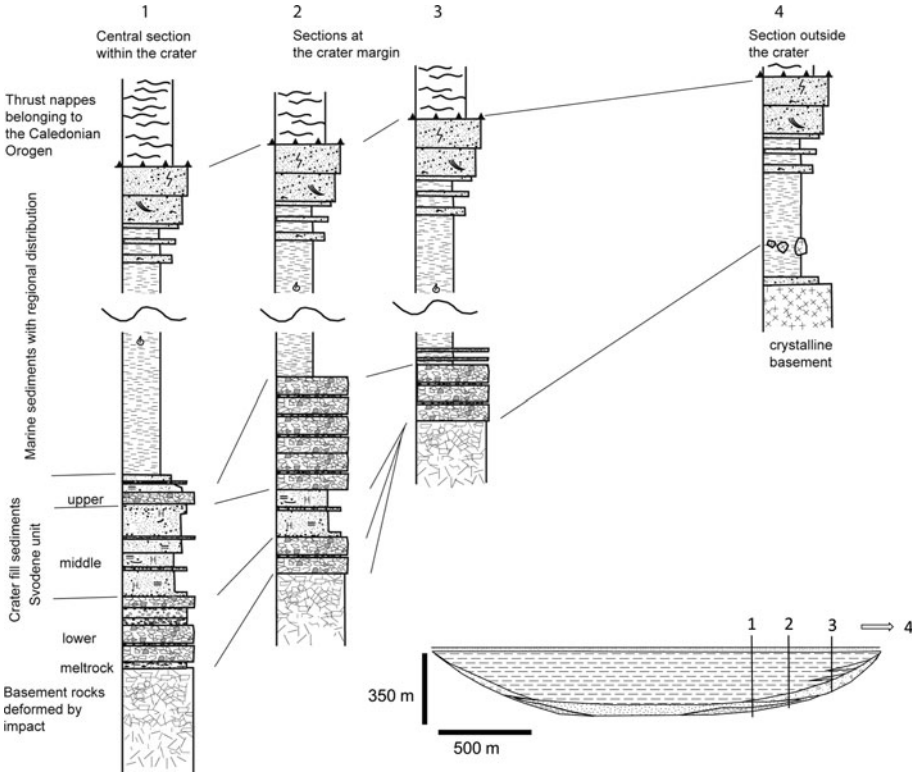

Fig. 2 The stratigraphical successions at Ritland. In the lowermost part of the sections crushed basement is shown, in *central* parts covered by about 2 m of melt–bearing rocks. The *lower* part of the sedimentary successions, the Svodene unit (~75 m), consists of early post-impact avalanche, slumps, mass flow- and suspension flow deposits. The overlying marine shales (~150 m) and sandstones (~10 m), represent Lower/Middle Cambrian sedimentation. Between the Cambrian sandstones and the overlying Caledonian nappes, a significant thrust zone is developed, truncating post-impact successions. The thrust zone is marked as a row of *black triangles* in the figure (modified from Riis et al. (2011)

an important basic question since most impacts on Earth are into marine targets. The SOVA model (Shuvalov 1999, 2003) handles this uniquely and it has, so far, only been used to model the Mjølnir and Lockne impacts (Shuvalov et al. 2005; Shuvalov and Dypvik 2004). In the Ritland case the sediment layer was thin and negligible, 10–12 m of clays, which probably were "blown away" immediately. The aim of this study was also to gain numerical information in order to aid ongoing geological investigations by theoretically illustrating crater evolution, sediment distribution and ejecta dispersion.

2 Numerical Model

The SOVA multi-material hydrocode (Shuvalov 1999) has been used to model shock wave propagation through water and solid target, transient crater growth, material ejection in a double layer (water and basement rocks) target, ejecta expansion and interaction with air and water ejecta curtain. The SOVA code has repeatedly been used for modeling impact phenomena (see, e.g., Shuvalov 2003; Shuvalov and Dypvik 2004; Artemieva and Morgan

2009; Shuvalov 2009). It is an Eulerian material response code with some Lagrangian features. SOVA allows considering strong hydrodynamic flows with accurate description of the boundaries between different materials (e.g., vapor, air, solid impactor substance, etc.). The governing transport equations consist of conservation equations of mass, momentum, and energy, which are solved for gas/liquid/solid phases (air, vapor, water, solid rocks). At the first step the Lagrangian equations are solved using a second-order difference scheme. At the second step the data is reinterpolated (remapped) from the Lagrangian grid to the Eulerian grid with the second order accuracy. The Van Leer (1977) second-order method is used for the remapping.

The table (Pierazzo et al. 2005) obtained with ANEOS equation of state (Thompson and Lauson 1972) for granite was used to describe thermodynamical properties of the target rocks and projectile material. The tabular equations of state described in Kuznetsov (1965) and Kosarev et al. (1996) were used to describe thermodynamical properties of the atmospheric air and sea water. A subroutine taking into account the influence of dry friction on the motion of disrupted rocks is used in the SOVA code to describe the cratering flow (impact induced motion of target material). It is based on the approach developed by Melosh and Ivanov (1999) applying a model of acoustic fluidization in the treatment by Ivanov and Turtle (2001).

Special efforts were undertaken to describe the expansion and deposition of basement ejecta taking into account its interaction with air and water (Shuvalov 1999, 2003). When any part of the ejected solid target material rises above the sea floor and its density decreases by a factor of two (with respect to the initial pre-impact density), it is considered to be ejected and transformed as discrete particles. The size distribution of the ejected material is defined from the data available for lunar land craters as described in Lindström et al. (2005). The largest ejected rock fragment size $d_{\max\_\max}$ is estimated as

$$d_{\max\_\max} = (25 \pm 12)\, D^{0.69\pm0.03}, \tag{1}$$

provided that the crater rim diameter, D, is measured in kilometers, and $d_{\max\_\max}$ is measured in meters. For the 2.7 km Ritland crater one can approximately obtain $d_{\max\_\max} = 50$ m. The size of the maximal ejecta fragment d_{max} is considered different for rocks ejected at different velocities:

$$d_{\max}(V) = d_{\max\_\max}\,(V_R/V), \tag{2}$$

where V is the launch velocity at some distance from the crater center, and V_R is an ejecta velocity near the transient crater rim:

$$V_R = [(4/15)\, g\, R_t]^{1/2}, \tag{3}$$

where g is the gravity acceleration. Assuming the radius of the transient cavity R_t for the Ritland crater to be about 1 km one can obtain $V_R = 50$ m/s.

The relation (2) is used to determine a value of $d_{\max}$ for each ejected volume. Then a standard presentation of the size distribution in the form (Melosh 1989)

$$N(m) = C_f m^{-b}, \tag{4}$$

is used. Here m is the mass of fragment, $N(m)$ is the cumulative number of fragments with mass equal or greater than m, and $b = 0.85$. The constant C_f is defined from the total mass of each ejected volume.

We consider six groups of particles with sizes: <0.1, 0.3, 1, 3, 10, and 30 m. Field investigations have, so far, disclosed ejecta blocks with sizes up to a few tens of meters

(Riis et al. 2011). Ejecta transportation can be described as motion of discrete particles, taking into account their interaction with surrounding air/water. Particles' motion, heat and momentum exchange with air/water flow are described in the frame of standard equations of multi-phase gasdynamics. To solve these equations a method of representative particles (markers) is used. Each marker describes the motion of great number (10^5–10^{10}) of real grains having similar velocities, sizes, temperatures and trajectories. In the Ritland simulations we used 20,000–30,000 representative particles.

Specially elaborated implicit algorithm provides correct solutions both for large boulders, which almost do not experience atmospheric drag and follow ballistic trajectories, and for small particles, which move with gas/water flow velocity. The method also provides a correct velocity of stationary deposition due to gravity (which depends on particle size). This procedure is described in more detail in (Shuvalov 1999, 2003), and in this case adopted for the specific Ritland target.

3 Results of Numerical Simulations

To perform 2D numerical simulations of the vertical impact we used a non-uniform computational grid consisting of 401 × 501 cells in R (radial) and Z (vertical) directions. The initial cell sizes h_r, and h_z were 1.25 m (46 cells across projectile radius). The cell size and the size of computational region were doubled when the shock wave reached the grid boundary. The doubling continued until the cell sizes reached maximum values of 10 m. This evolution of the grid allowed us to describe all stages of the impact with approximately the same, rather high spatial resolution.

The projectile is considered to be a 115-m-diameter granite sphere impacting the Earth at a velocity of 18 km/s (115-m in diameter projectile was selected to fit the 2.7 km in diameter crater size, while the 18 km/s is an average asteroid impact velocity). The real composition of the projectile and its structure is not known, but most likely, the projectile was strongly deformed/fragmented before the impact. On the other hand the numerical simulations show that impact process is dominated by projectile energy. For this reason we used the same equation of state for both target and projectile, which simplifies the numerical procedure. The thin ($\sim$10–12 m) layer of marine shale (clays at the time) overlying the basement is very important for reconstruction of paleogeographic setting, implying that a shallow sea had transgressed the peneplanated basement at time of impact. However, being very thin and soft, it had probably negligible effect on the crater formation and was probably mostly "blown away" during impact. It has not been included as a separate layer in the numerical simulation. To study the influence of water layer we performed numerical simulations of the impact for three values of sea depth: H = 0 (no water), 100, and 200 m. Input data are summarized in Table 1.

Figure 3 shows the evolution of a crater for H = 100 m. 1 s after the impact one can see a growing basement crater, a transient water cavity of the same diameter, and initial ejecta curtain consisting of both water and solid fragments. Approximately 7 s after the impact the excavation stops, the transient crater reaches its maximum depth and diameter. In an upper part of the ejecta curtain one can see a separation of ejecta by particle sizes, large rock fragments experience a relatively lower drag and move faster than small ones. In general this shallow water cratering compare fairly well to a dry, subaerial impact. The next state (t = 25 s) illustrates processes of crater modification under gravity (slumping of crater walls of crushed crystalline-rock). Ejecta separation by particle sizes becomes even more pronounced and large blocks begin to fall into the surrounding sea. Approximately

Table 1 Input data for the numerical simulation

Granite density	2,630 kg/m^3
Cohesion	0
Friction	0.7
Shock modification pressure (PDFs)	4 GPa
Melting pressure	50 GPa
Porosity	0 %
Water density	1,000 kg/m^3
Impact velocity	18 km/s
Initial spatial resolution	46 ppr
Projectile diameter	115 m
Water depth	0, 100, 200 m

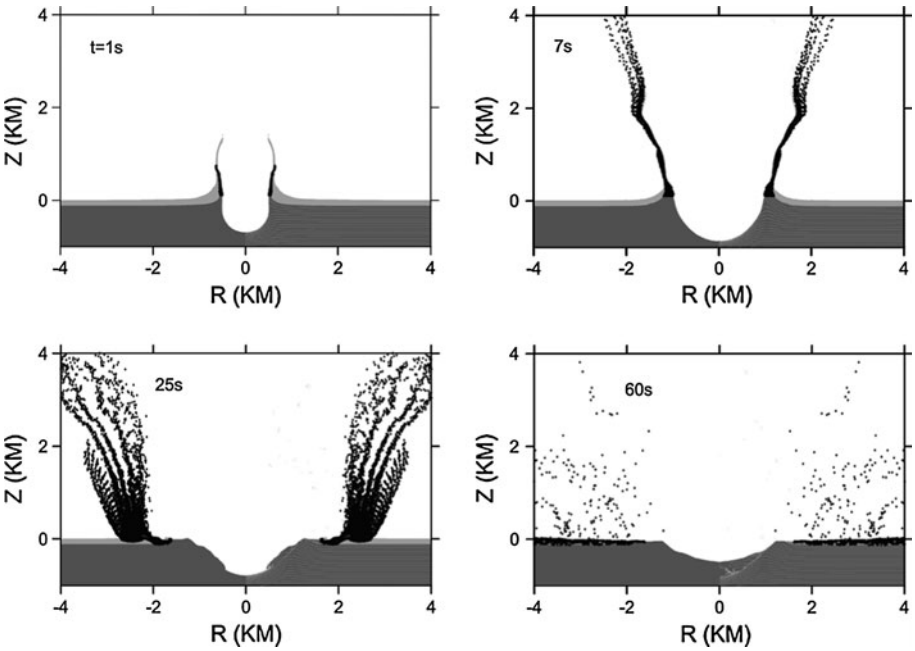

Fig. 3 Evolution of the transient crater and ejecta curtain after a vertical impact of a 115-m-diameter granite projectile into a sea 100 m deep. Time steps 1–60 s are shown. *Light gray lines* show impact induced displacement of original horizontal platform layers, *black dots* show basement ejecta particles. *Light gray shading marks* sea water, *dark gray shading marks* solid target material. The *dot size* does not correspond to particles' sizes; the *dots* show only positions of the particles. Only suspended (not deposited) particles are shown. 7 s after the impact the transient crater reaches its maximum volume, 25 s time step shows a process of crater modification, and the last *image* shows a modified crater (not disturbed by possible resurge)

1 min after the impact the basement crater reaches its final shape. Minor changes will continue to appear, resulting from e.g. the interaction of the sea water and the rim walls. The height of the crater rim is comparable with the sea depth, consequently return of seawater (resurge flow) and crater filling with water should be rather slow. In this situation the resurge flow depends very strongly on the rim height, which is not determined very accurately in our modeling. For this reason we did not consider the resurge. At this moment

Fig. 4 Evolution of the transient crater and ejecta curtain after a vertical impact of a 115-m-diameter granite projectile into the sea 200 m deep. Time steps 1–180 s are shown. *Light gray lines* display impact induced displacement of the original horizontal platform layers; *black dots* show basement ejecta particles. *Light gray shading marks* sea water, *dark gray shading marks* solid target material. The *dot size* does not correspond to particles' sizes, the *dots* show only positions of the particles. Only suspended (not deposited) particles are shown. 7 s after the impact the transient crater reaches its maximum volume, 15 and 25 s time steps show a process of crater modification, 40 s time step shows modified crater and beginning of the resurge, and the last images (40–180 s) demonstrate processes of crater filling ▶

most of the ejecta falls into the sea and its further evolution and deposition is defined by sediment/water interaction. The cratering flow at the 100 m water depth scenario is comparable to other shallow water marine impacts, e.g. the Mjølnir impact (Shuvalov et al. 2002). In this case the water layer very slightly influences the cratering process and final crater.

Figure 4 shows the evolution of water and basement craters after an impact of the same projectile (granite composition, 115 m diameter, 18 km/s) hitting a 200 m deep sea. Separated water and basement ejecta curtains are formed a few seconds after the impact and separated water and basement cavities are developed (state $t = 1$ s). The horizontal size of the water cavity exceeds that of the basement crater, consequently basement ejecta strikes the walls of water transient crater and smaller particles are decelerated and move within the water ejecta curtain. Large fragments could penetrate through the water ejecta curtain but with decreased velocities. Smaller ejecta fragments decelerate within the water ejecta curtain and for some time move with approximately the same velocity as ejected water. Later ($t > 10$–15 s) one can see a considerable separation between water and solid ejecta and separation of particles by sizes. The water therefore, in this case, strongly restricts the distribution of basement ejecta. The height of the basement ejecta curtain is reduced compared to the 100 m water depth case as shown in the 15 s and 25 s time steps of Fig. 4, and large fragments will land after a short flight as shown in time step 40 s. Approximately 1 min after the impact most ejecta with sizes exceeding 10 cm landed in a 200 m deep sea (see time step 65 s of Fig. 4).

In the case of the 200 m water depth scenario, the height of the crater rim (about 100 m) is considerably (by one half) less than the water depth and intensive resurge flows are formed, starting after end of crater modification stage (slumping of crater walls). The resurge flow will transport some ejecta and crushed rock fragments suspended in water into the crater. 2–3 min are needed to fill the crater with water, approximately comparable time is needed for large, reworked, ejecta fragments (with sizes exceeding 10 cm) to pass through the water column and settle on the crater floor.

Figure 5 compares basement transient craters on land to deeper water depths and shows the influence of decreasing crater depth as depth of sea water increases. The resulting crater diameter is approximately the same in all three alternatives because of rather small water depth under consideration.

Figure 6 illustrates a distribution of ejecta deposits around the crater. For comparison an analytical approximation

$$\delta = 0.04 R_t \, (R/R_t)^{-3.5} \tag{5}$$

from Melosh (1989) is also shown in this figure. Here δ is a thickness of ejecta blanket, in meters. The approximation correlates well with the results of simulations for the impact on land. The presence of water considerably decreases the thickness of the ejecta blanket and restricts area of ejecta deposits. In the case of 100 m water depth most of the ejecta precipitates at distances less than approximately 17 km, while with 200 m of water depth

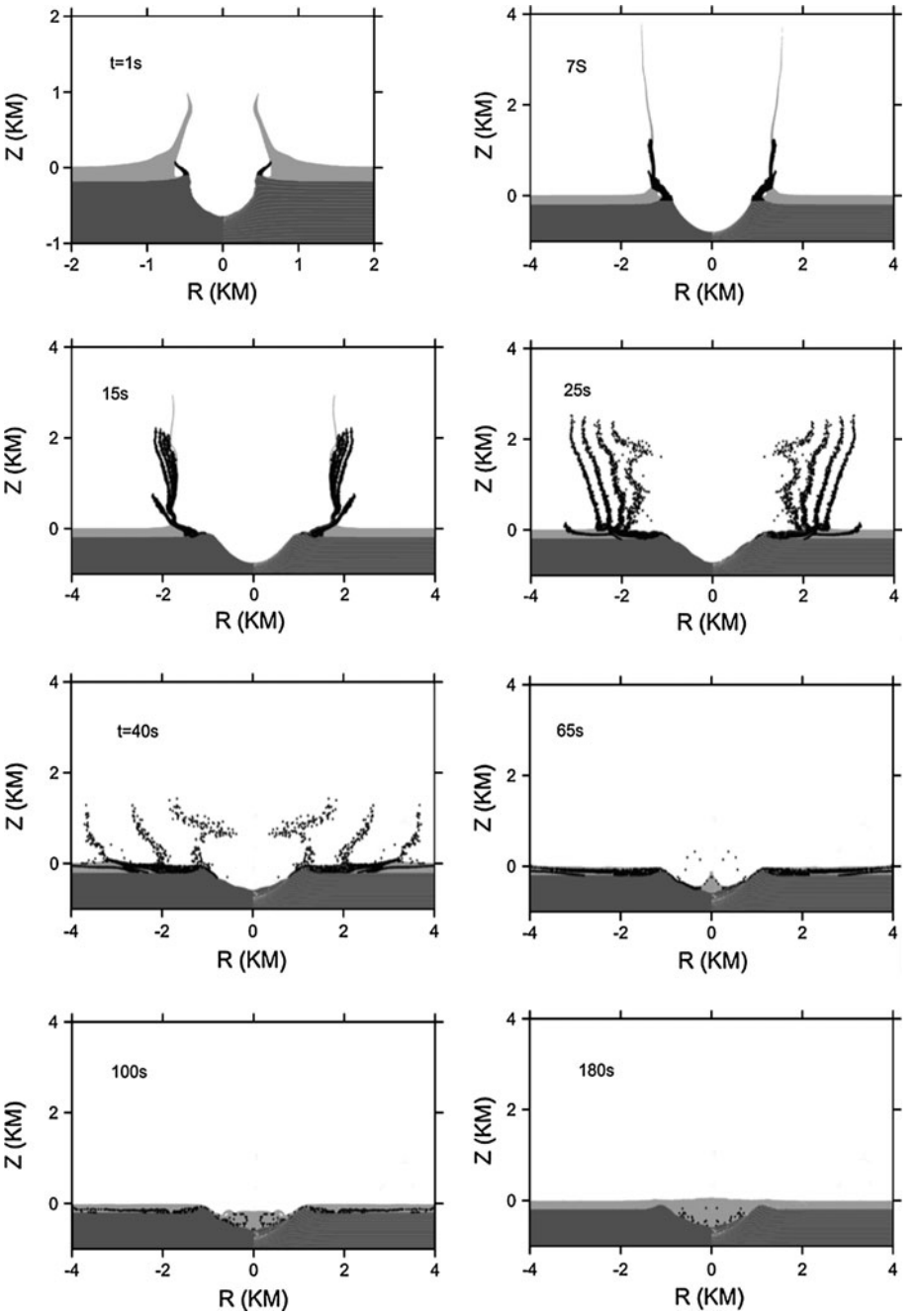

the area of ejecta deposits is restricted to a distance of about 6 km. It should be mentioned that very small particles (with sizes 1 mm and less) will be suspended in the air for a long time (hours and even days) and could travel for long distances depending on e.g. weather conditions.

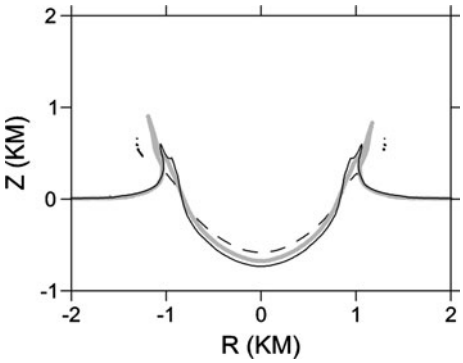

Fig. 5 Comparison of basement transient craters (7 s after the impact) for impacts of a 115-m-diameter stony projectile on land (*black line*) and into the sea 100 (*thick gray line*) and 200 (*dashed line*) meters deep. Depth/height Z is measured from the top surface of solid target

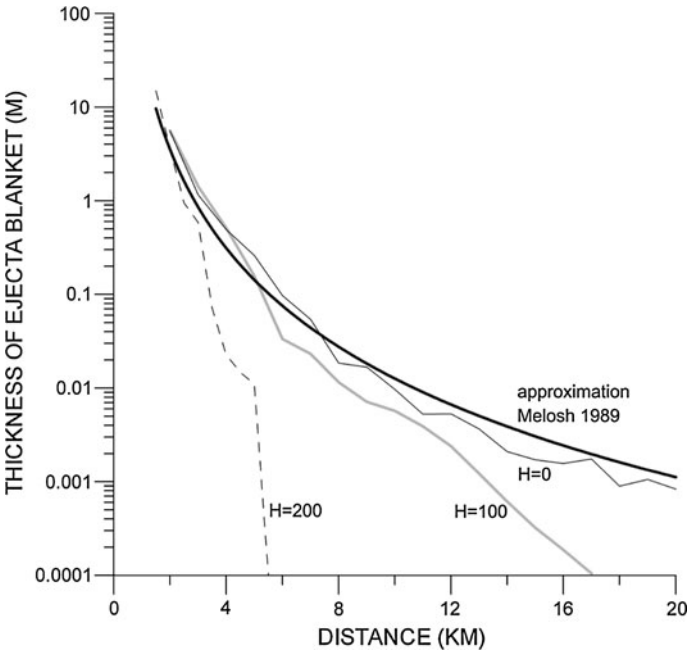

Fig. 6 Modeled ejecta layer thickness versus distance R from the crater center. The *thin black line* corresponds to the impact on land, *thick gray and dashed lines* correspond to impacts into the sea 100 and 200 m deep, *thick black line* corresponds to approximation from Melosh (1989)

The numerical simulations show that large blocks of ejecta (10 m and larger) could be transported as far as 6 km, if water depth equals 100 m or less. In the 200 m water depth alternative such large blocks of ejecta are shown to travel for distances up to 4 km only. Figure 7 illustrates the shock compression of target material during the impact. More than 1,000 M (M = projectile mass) of target rocks experience overpressure above 4 GPa, which is the level of main microscopic shock metamorphism features like PDFs (Stöffler and Langenhorst 1994). This level changes with water depth (H): from 1,500 M for H = 200–2,500 M for H = 0. Shock melting of target rocks (consisting dominantly of granite) starts from overpressure of about 50 GPa. The mass of target rocks compressed

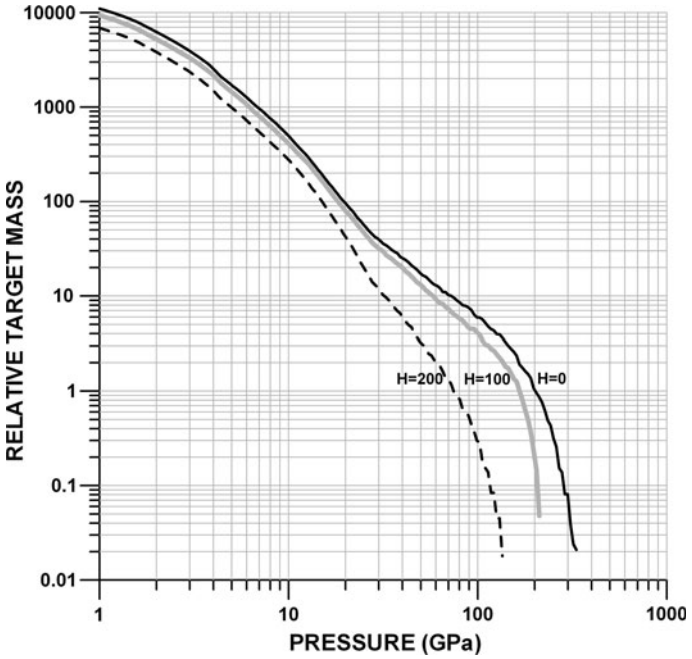

Fig. 7 Graph showing the effects of water depth on the amount of shock modified target material. Relative target mass (measured in projectile masses M) shock-compressed above pressure p versus pressure p. The *thin black line* corresponds to the impact on land, *thick gray and dashed lines* correspond to impacts into a 100 and 200 m deep sea, respectively

above this pressure equals 3 M, 13 M, and 18 M for H = 200 m, H = 100 m, and H = 0 correspondingly.

In the 200 m water depth scenario the resurge water velocity reaches 30 to 40 m/s within the crater and 5–10 m/s outside the crater (Fig. 8). The outwards water velocity behind the first tsunami-like wave reaches 10–20 m/s. The typical time of intensive water motion is some 100 s. This means that ejecta fragments could be displaced by water flow for a distance of about 0.5–1 km in the area outside the crater and for a distance of about crater size within the crater. In the 100 m water depth alternative we know nothing about the resurge because it very strongly depends on an exact value of the rim height (which in this case is close to the water depth H) (Fig. 9). The outwards water velocity behind the first tsunami (about 15–25 m/s) is even somewhat higher in the 100 m water depth alternative (Fig. 9).

4 Discussion and Conclusion

During Early/Middle Cambrian times the sub-Cambrian peneplain of southern Norway was transgressed and a shallow epicontinental sea established. Based on Nielsen and Schovsbo (2006) a shallow water depth of this sea in the study area is likely, supporting an interpretation that it was probably below 100 m. According to the appearance of the dark gray laminated shale lithologies, the setting was dominated by high organic production and possible hypoxic bottom water conditions.

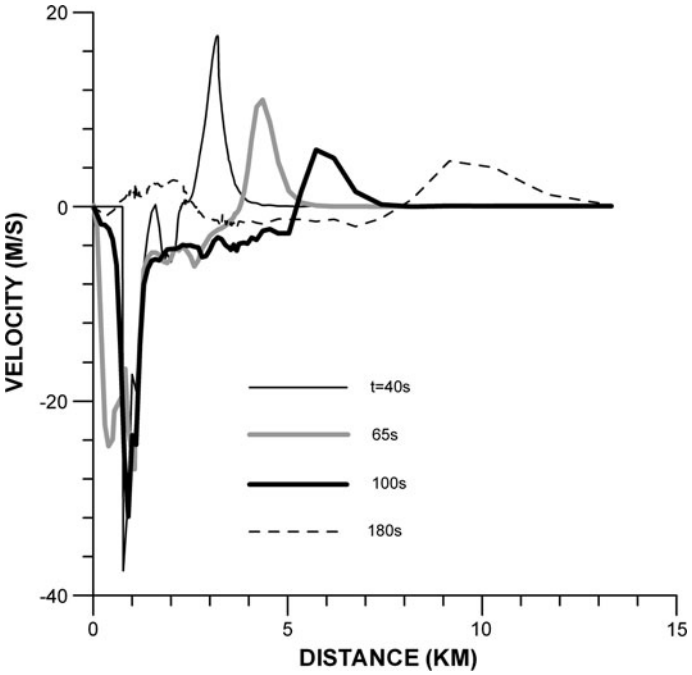

Fig. 8 Horizontal water velocity versus distance from crater center for different moments of time t for the Ritland impact event (at the 200 m water depth scenario). Positive velocity values correspond to the outward flow; negative velocities are directed to the crater center

Detailed field observations and supporting laboratory analysis (petrography, mineralogy) indicate an about 2.7 km crater, with crater infill successions characterized by avalanche, slump and mass flow deposits from a syn-impact/early post-impact phase, while fine-grained dark gray clays were deposited thereafter (Riis et al. 2011). The simulations show a 115 m bolide at an impact velocity of 18 km/s in 100 m of water could explain the Ritland structure geometry. According to the simulation ejecta blocks up to 10 m in diameter could be transported up to 6 km and ejecta particles of larger than sand size were deposited up to 17 km away from the crater. These sizes are much greater than was observed in the field, however (the largest observed clast size is up to about 20 cm at a distance of 5–6 km from the crater center (Kalleson et al. in preparation). In locations east of the crater (Setså 2011; Kalleson et al. 2012) ejecta material is found in a stratigraphic level within the Lower/Middle Cambrian shales of the area, about 10 m above the peneplanated basement surface. Precise biostratigraphic dating of this level is not available and demands much more field work.

The appearance of sporadic carbonate cement in the sedimentary succession along with the depth estimations of Nielsen and Schovsbo (2006), make a shallow, less than 100 m water depth most likely for the impact site. According to the presented numerical impact model of this water level the crater rim (about 100 m in height) formed a serious obstacle and hampered resurge filling of the crater, since water depth most likely was shallower than about 100 m. Consequently, while the crater formed in about 1 min, the water-return must have taken more time, due to the damming of the water by the crater rim. The simulations demonstrate probable water resurge velocities of 30–40 m/s (for water depth

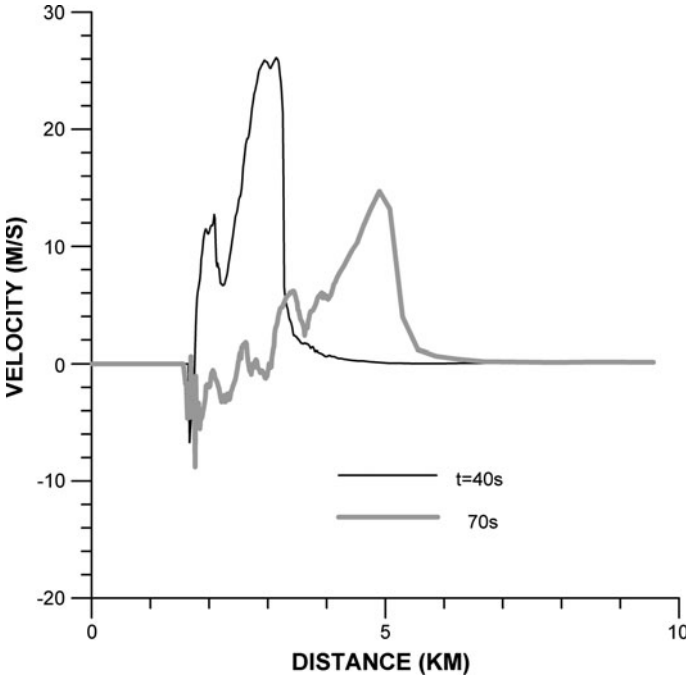

Fig. 9 Horizontal water velocity versus distance (from crater center) for 40 and 70 s for the Ritland impact event (at the 100 m water depth scenario). Positive velocity values correspond to the outward flow; negative velocities are directed to the crater center

H = 200 m), powerful enough for important displacement of particles both outside and inside the crater. If, alternatively, the water depth was deeper at the impact site, more powerful resurge processes; tsunami wave generations and related currents would have been expected to be active and triggered more violent and fluidal controlled sedimentation. This will be tested in ongoing analyses of the sedimentary syn- and post impact successions (Azad et al. 2012). It is likewise possible that coarse grain sedimentation dominated along the margins while more fine grained clays should be expected in the central parts of the crater basin. In western and central parts of the Ritland structure possible postimpact deposits have been eroded and transported away by other, much younger geological events (e.g. Quaternary glaciations).

The well-exposed and easy accessible Ritland crater is very well suited for studies combining field analysis and numerical modeling. These are iterative processes which benefit from each other. The presented numerical model will clearly function as a tool to aid the ongoing geological investigations of crushed basement, crater rim, sedimentary syn- and postimpact crater fill successions and ejecta.

Our numerical simulations demonstrate the most typical features of marine target impacts:

- increasing water depth causes decreasing basement crater depth;
- deeper water more strongly restricts ejecta distribution;
- mass of shock modified target rocks decreases with deeper water and increases with shallower water;
- velocities of resurge flow are higher than velocities of outward flow;

- most of the ejecta (except centimeter-sized or smaller particles) settles within a few minutes (depends on water depth).

Impact into marine targets, so-called subaquatic impacts, should be the most common on the Earth. Consequently studies of the effects of water in impact cratering will be of great general importance; in this case the new numerical simulation in particular demonstrates the influence of water depth of the impact site on ejecta distribution and on the resurge of the water into the crater.

Acknowledgments The Ritland project group members are thanked for good discussions and great days in field and lab. The Research Council of Norway has kindly supported The Ritland Project. The detailed comments of Alex Deutsch and an anonymous referee are highly appreciated.

References

A.S. Azad, H. Dypvik, E. Kalleson, F. Riis, LPSC 2012. Abstract # 1281 (2012)
N. Artemieva, J. Morgan, Icarus **201**, 768 (2009)
J.A. Dons, J. Naterstad, Meteoritics **27**, 215 (1992)
H. Dypvik, J. Plado, C. Heinberg, E. Håkansson, L.J. Pesonen, B. Schmitz, S. Raiskila, Episodes **31**, 107 (2008)
B.M. French, C. Koeberl, I. Gilmour, S.B. Shirey, J.A. Dons, Geochim. Cosmochim. Acta. **61**, 873 (1997)
S. Goderis, E. Kalleson, R. Tagle, H. Dypvik, R-T. Scmitt, J. Erzinger, P. Claeys, Chem. Geol. **258**, 145 (2009)
B.A. Ivanov, E.P. Turtle, LPSC 2001. Abstract # 1284 (2001)
E. Kalleson, F. Corfu, H. Dypvik, Geochim. Cosmochim. Acta **73**, 3077 (2009)
E. Kalleson, H. Dypvik, J. Naterstad, Postimpact sediments in the Gardnos impact structure, Norway. In: *The Sedimentary Record of Meteorite Impacts*, ed. by K.R. Evans, J.W. Horton Jr., D.T. King Jr., J.R. Morrow, Geological Society of America Special Paper 437 (2008), p. 19
E. Kalleson, F. Riis, R. Setså, H. Dypvik, LPSC 2012. Abstract # 1351 (2012)
I.B. Kosarev, T.V. Loseva, I.V. Nemtchinov, Sol. Syst. Res. **30**, 265 (1996)
N.M. Kuznetsov, *Thermodynamic Functions and Shock Adiabats for Air at High Temperatures* (Mashinostroyenie, Moscow, 1965), p. 464. (in Russian)
M. Lindström, V. Shuvalov, B.A. Ivanov, Planet. Space Sci. **53**, 803 (2005)
H.J. Melosh, *Impact Cratering: A Geologic Process* (Oxford University Press, NY, 1989)
H.J. Melosh, B.A. Ivanov, Annu. Rev. Earth Planet. Sci. **27**, 385 (1999)
A.T. Nielsen, N.H. Schovsbo, Bull. Geol. Soc. Denmark **53**, 47 (2006)
E. Pierazzo, N. Artemieva, B. Ivanov, Starting conditions for hydrothermal systems underneath Martian craters: Hydrocode modeling. In: *Large Meteorite Impacts III*, vol. 443, ed. by T. Kenkmann, F. Hörz, A. Deutsch, Geological Society of America Special Paper 384 (2005)
F. Riis, E.Kalleson, H. Dypvik, S.O. Krøgli, O. Nilsen, Meteorit. Planet. Sci. 14 (2011). doi: 10.1111/j.1945-5100.2011.01188x
F. Riis, H. Dypvik, E. Kalleson, LPSC 2012. Abstract # 1353 (2012)
R. Setså, The Ritland impact structure: characteristics and distribution of the ejecta layer and associated Lower Paleozoic sedimentary succession. MS Thesis University of Oslo (2011), 109 pp
V. Shuvalov, Shock Waves **9**, 381 (1999)
V. Shuvalov, Displacement of target material during impact cratering, in *Impact Markers in the Stratigraphic Record. ESF Impact Series 2003*, ed. by C. Koeberl, F.C. Martinez-Ruiz (Springer, Berlin, 2003), pp. 121–135
V.V. Shuvalov, Meteorit. Planet. Sci. **44**, 1095 (2009)
V. Shuvalov, H. Dypvik, Meteorit. Planet. Sci. **39**, 467 (2004)
V. Shuvalov, J. Ormö, M. Lindström, In: *Impact Tectonics. ESF Impact Series 2005*, ed. by C. Koeberl, H. Henkel (Springer, Berlin, 2005), pp. 405–422. doi:10.1007/3-540-27548-7_16
V. Shuvalov, H. Dypvik, F. Tsikalas, J. Geophys. Res. **107**(7), 1-1–1-13 (2002). doi:10.1029/2001JE001698
D. Stöffler, F. Langenhorst, Meteoritics **29**, 155 (1994)
S.L. Thompson, H.S. Lauson, *Improvements in the Chart D Radiation-Hydrodynamic CODE III: Revised Analytic Equations of State*. Report SC-RR-71 0714 (Sandia National Laboratory, Albuquerque, New Mexico, 1972), 119 pp
B. Van Leer, Comput Phys **23**, 276 (1977)